

Journal of Materials Chemistry A

Accepted Manuscript



This is an *Accepted Manuscript*, which has been through the Royal Society of Chemistry peer review process and has been accepted for publication.

Accepted Manuscripts are published online shortly after acceptance, before technical editing, formatting and proof reading. Using this free service, authors can make their results available to the community, in citable form, before we publish the edited article. We will replace this *Accepted Manuscript* with the edited and formatted *Advance Article* as soon as it is available.

You can find more information about *Accepted Manuscripts* in the [Information for Authors](#).

Please note that technical editing may introduce minor changes to the text and/or graphics, which may alter content. The journal's standard [Terms & Conditions](#) and the [Ethical guidelines](#) still apply. In no event shall the Royal Society of Chemistry be held responsible for any errors or omissions in this *Accepted Manuscript* or any consequences arising from the use of any information it contains.

ARTICLE

Tin microparticles for a lithium ion battery anode with enhanced cycling stability and efficiency derived from Se-doping

Cite this: DOI: 10.1039/x0xx00000x

Received 00th January 2012,
Accepted 00th January 2012

DOI: 10.1039/x0xx00000x

www.rsc.org/

Hoang X. Dang,^a Kyle C. Klavetter,^a Melissa L. Meyerson,^a Adam Heller,^a and C. Buddie Mullins^{ab*}

In a 100 cycle test at 0.5 C-rate a negative electrode formed of micro-sized Sn_{0.9}Se_{0.1} particles retains a specific capacity of 500 mAh/g with a coulombic efficiency of 99.6%. In contrast, a control electrode made with pure Sn retains only a 200 mAh/g capacity with a 98.7% efficiency. The improvement in electrochemical performance of the Sn/Se alloy is attributed to the reduced inactive Se-phase preventing agglomeration of Sn to a size susceptible to particle fracture. The Sn/Se alloy particles are manufacturable, being made by melting the 9:1 atomic ratio mixture of Sn and Se, quenching and jet-milling.

Introduction

Sn-based alloys have been studied as graphite-alternative materials for the development of more safe and higher energy density lithium-ion anodes. Sn-based alloys are attractive because of their high theoretical capacity and energy density of 2094 Ah/L and 4.2 kWh/L (for the charged Li_{4.4}Sn phase, similar to that of Li_{4.4}Si, 2213 Ah/L).¹ Tin is also non-toxic, abundant and inexpensive. However, the strain resultant from the 258% volume change of Sn upon charging/discharging²⁻⁵ leads to particle fracture and to rapid loss of specific capacity. Particle fracture has been alleviated by nano-structuring the active Sn phase so long as the individual particles remain segregated. Because the melting point of tin is only 232°C, the small particles tend to either coalesce or if their coalescing is prevented by a chemically stable electrolyte interface (SEI), they lose coulombic efficiency.^{4, 6-8} Nano-structured particles have low tap density and lead to lower energy density anodes, making scale up difficult.⁹⁻¹³ The adverse morphological changes upon cycling have also been alleviated by embedding the tin in a carbon matrix,¹⁴⁻¹⁸ alloying with copper,^{19, 20} nickel,²¹ cobalt²² and germanium,²³⁻²⁵ and compound formation with chalcogenides, the compounds including SnSe,²⁶⁻²⁸ SnS²⁹ and their formulated mixtures, e.g. Sn-SnS-C.³⁰

Here we apply the strategy of mixing a small fraction of a non-cycling Se phase (optimized to 10 at% Se) with Sn to stabilize a microparticle rather than nanostructured material. The advantages of this Sn_{0.9}Se_{0.1} microparticle include its production by a scalable jet-milling technique,³¹ high tap density and low specific surface area which allows for slurry casting of a high energy density electrode. To the best of our knowledge, this is the first report demonstrating significantly

increased cycling stability and coulombic efficiency for a Sn-based micron-sized particle.

This combinatorial study of a Sn-Se active material was motivated by the findings from recent studies of thin film³² and high tap density³³ germanium sub-selenide anodes. In these studies considering both nano- and micro-structured active material morphologies, the mixture of a sub-stoichiometric amount of chalcogenides with a group IV element was observed to consistently improve the coulombic efficiency and cycling stability. By incorporating small mole fractions of the electrochemically inactive phase, first cycle irreversible losses were minimized and the intrinsically high capacity of the particle was largely preserved. The electrochemical improvements resulting from the inclusion of a sub-stoichiometric chalcogenide inactive phase were attributed to a combination of the inactive phase alleviating the strain and enhancing solid state lithium diffusion.

In the Sn-Se mixture studied here, we believe that the reduced Se species, Li₂Se or a thermodynamically more stable Li-Se-Sn phase should such a phase exist, buffers against the volumetric changes of Sn within the microparticle during cycling, thereby allowing for stabilized electrode performance. It may also be that solid state lithium diffusion is enhanced through this inactive phase or by the grain boundaries introduced by its inclusion in the majority-Sn microparticle.

Experimental

Synthesis

The micron-sized Sn/Se particles were prepared by melting mixtures of powders of 99.9% Sn (Alfa Aesar) and Se 99.99% (Lesker) of Sn/Se atom ratios of 9.0/2.0, 9.0/1.0, 9.0/0.5 in an

evacuated quartz ampoule at 1100°C, rocking the melt for 40 hrs in a rocked tube furnace (Blue M, single zone, Lindberg). The ampoule was quenched by dropping it into an ambient temperature water bath. The resulting ingots were manually crushed in a mortar and jet-milled (Jet-O-Mizer, Fluid Energy). The resulting powder was sieved with a #325 mesh.

Characterization

X-ray diffraction (XRD) patterns were acquired with a Spider (Rigaku) diffractometer using Cu K α radiation employing the detector scan mode with an incident angle of 2° at a scan rate of 3°/min. X-ray diffraction patterns used for estimating grain size were acquired using a Rigaku Miniflex. Scanning electron (SEM) images and energy dispersive x-ray spectra (EDS) were acquired with a Hitachi S-500 at 30 kV accelerating voltage.

Electrochemical testing

Electrodes were made of an 8:1:1 aqueous slurry of the Sn/Se particles or of purchased Sn microparticles (#325 mesh, Alfa Aesar), carbon black (Super P-Li, Timcal) and 90 kDa sodium carboxymethyl cellulose (Sigma Aldrich). Because un-alloyed Sn is soft, it cannot be processed by jet milling into microparticles as it deforms rather than fracturing during its milling. The slurry was cast on a 10 μm thick Cu foil using an automatic film applicator. The Cu foil loaded typically with $\sim 700 \mu\text{g}/\text{cm}^2$ of the particles, was dried *in vacuo* at 80°C for 12 hrs, then punched into 7/16 inch diameter disks. Employing an argon-atmosphere glove box (MBraun Unilab) the electrode disks were assembled in 2032 coin cells having Li-metal (Alfa Aesar, 99%) counter electrodes, a 1M LiPF₆ (Sigma-Aldrich, battery grade) in a 1:1 v:v solution of fluorinated ethylene carbonate (Solvay Chemicals) and diethyl carbonate (Sigma Aldrich, battery grade) electrolyte, and a Celgard 2400 polypropylene membrane separator. The cells were cycled, typically between 10 mV and 1.2 V vs. Li/Li⁺, using a multichannel battery tester (BT2043, Arbin). Exhaustively cycled electrodes were recovered from cells disassembled in the glove box and kept in the DEC overnight to strip their LiPF₆. To remove the SEI layer of the cycled electrode area shown in Fig.9, the cycled electrode was disassembled from the coin cell and soaked in acetonitrile for 24 h, then rinsed with ethanol to remove the residual electrolyte, followed by drying under vacuum at 80°C overnight before SEM imaging.³⁴

Results and discussion

Material characterization

In this study, different Se-doped Sn samples are referred to by their prepared atomic ratio of Sn to Se. Thus, samples Sn/Se(9/2), Sn/Se(9/1), Sn/Se(9/0.5) correspond to powders prepared with Sn/Se atomic ratios of 9.0/2.0, 9.0/1.0, and 9.0/0.5, respectively.

Selenium effectively hardens the tin; even a small atom fraction of Se abruptly raises the melting temperature³⁵ and allows for the Sn-based particle to be processed by jet milling.

At the Sn/Se = 9/1 atom ratio, the melting temperature increases to $\sim 750^\circ\text{C}$ from 232°C for pure Sn.

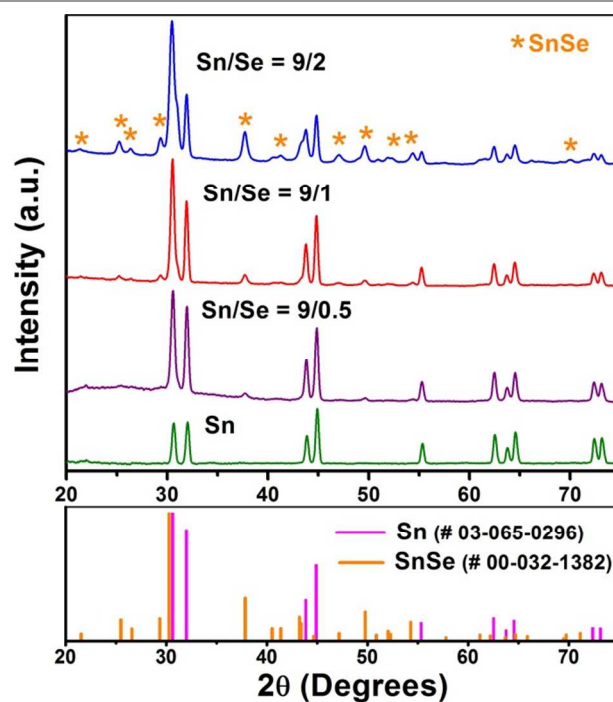


Figure 1. XRD patterns of Sn/Se particles at various Sn/Se atomic ratios, and commercial Sn (# 325 mesh) particles..

XRD patterns of the studied Sn/Se compositions (Fig. 1) show the presence of SnSe, its 37.8° peak intensity increasing relative to those of Sn, as expected, with the Se atom fraction. SEM images (Fig. 2) show that the jet milled and sieved powders consist mostly of micron-sized particles, with some sub-micron fines.

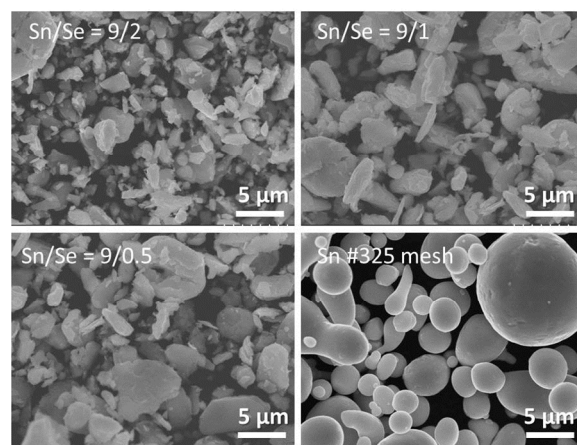


Figure 2. SEM images of Sn/Se particles at various Sn/Se atomic ratios, and commercial Sn (# 325 mesh) particles.

The uniform elemental distribution within Sn/Se(9/1) particles is demonstrated in Fig. 3(a-d). This result is expected given the formation of a single liquid phase during the synthesis. Fig. 3e is a typical spectrum for a line scan across a Sn/Se(9/1) particle.

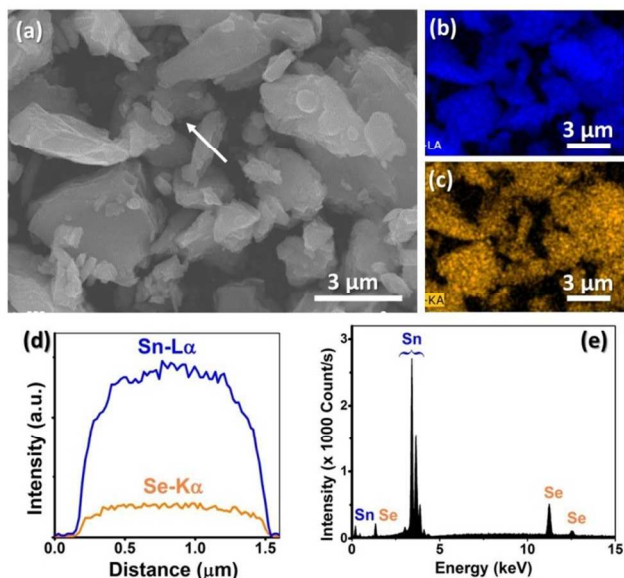


Figure 3. (a) SEM of Sn/Se(9/1), the arrow pointing to the EDS line-scanned particle. (b) Sn EDS; (c) Se EDS. (d) Sn and Se scans across the particle of (a) particle; and (e) the corresponding spectrum.

Point scans along the scan line revealed the elemental ratio of Sn/Se to be $\sim 9.0/1.0$ as expected from the starting composition. This is also the case for the 9:0.5 and the 9:2 atomic ratio compositions. (Supporting Information Fig. S1 and S2). This observation suggests the advantage of the current method in preparing uniform Sn/Se composites with pre-determined elemental ratios. All the Sn/Se and Sn powders were then slurry-cast to the corresponding anodes to investigate the effect of selenium content on lithium storage performance.

Lithium storage performance

Fig. 4a shows the retention of the reversible gravimetric capacities of anodes made with powders of various Sn/Se atomic ratios and pure Sn micro particles.

Of the four electrodes, the Sn/Se(9/1) electrode had the highest reversible capacity, slightly greater than 500 mAh/g after 100 cycles, while the Sn/Se(9/2) electrode was the most stable, retaining better its slightly lesser starting capacity (because Li_2Se does not cycle). All three electrodes substantially out-performed the pure Sn electrode, which retained only a 200 mAh/g capacity at the 100th cycle. The Columbic efficiencies of the Sn/Se(9/2) and Sn/Se(9/1) electrodes exceed those of the Sn/Se(9/0.5) and pure Sn electrodes. At the 100th cycle the Columbic efficiencies for 9/2, 9/1, 9/0.5 atomic ratio Sn/Se and Sn electrodes are 99.7 %, 99.6 %, 99.3 % and 98.7 %, respectively.

Comparison of the first charging half-cycle voltage profiles of an un-doped Sn electrode (solid green line, Fig. 5b) with the first charging half-cycle voltage profiles of the three Se doped electrodes (Fig. 5a solid blue and solid violet lines and 5b solid red line) show Se-associated irreversible capacities at voltages greater than 0.7 V, and Sn-associated reversible capacities at voltages less than 0.7 V.

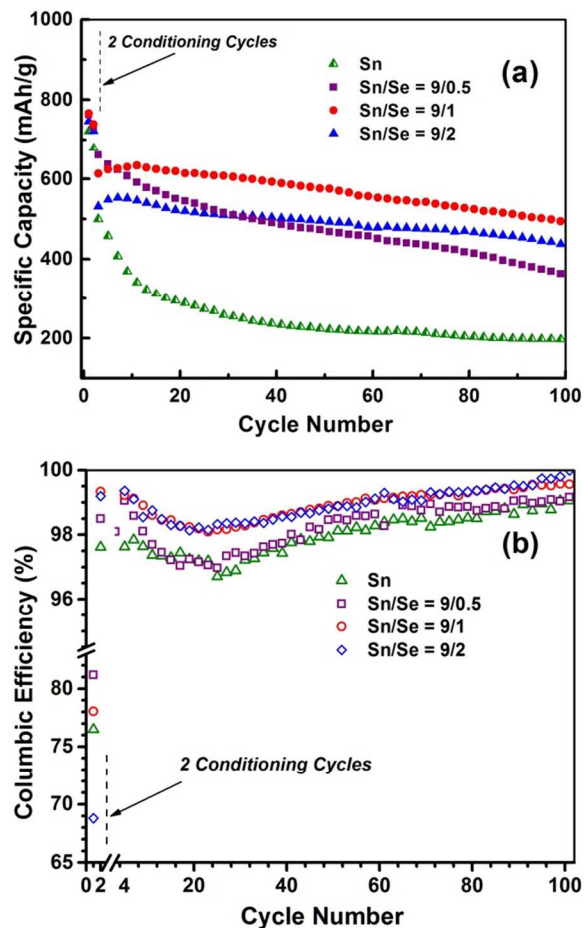


Figure 4. Retention of the reversible capacities of the electrodes made with Sn/Se and Sn particles when cycled at 0.5 C rate (496 mA/g). The cells were conditioned by two 0.05 C rate cycles prior to their cycling at the 0.5C rate. In computing the specific capacity both the mass of Sn and Se in the electrode were employed.

The reversible lower voltage capacities are attributed to the lithiation of Sn whereby well-known Li_xSn alloys are formed.^{8, 36} At voltages greater than 0.7 V, particularly near 1.25 V, the reduction of the SnSe phase to Li_2Se or a thermodynamically more stable Li-Se-Sn phase, should such a phase exist, is observed (Reaction 1, Fig 5c). The reduction of SnSe at near 1.25 V has been reported previously as forming Li_2Se .^{28,37, 38,39}

The intensities of the 1.25 V differential capacity peaks (Fig. 5c), and the corresponding high voltage specific capacities, increase, as expected, with the atom fraction of Se; they are nil in the absence of Se.

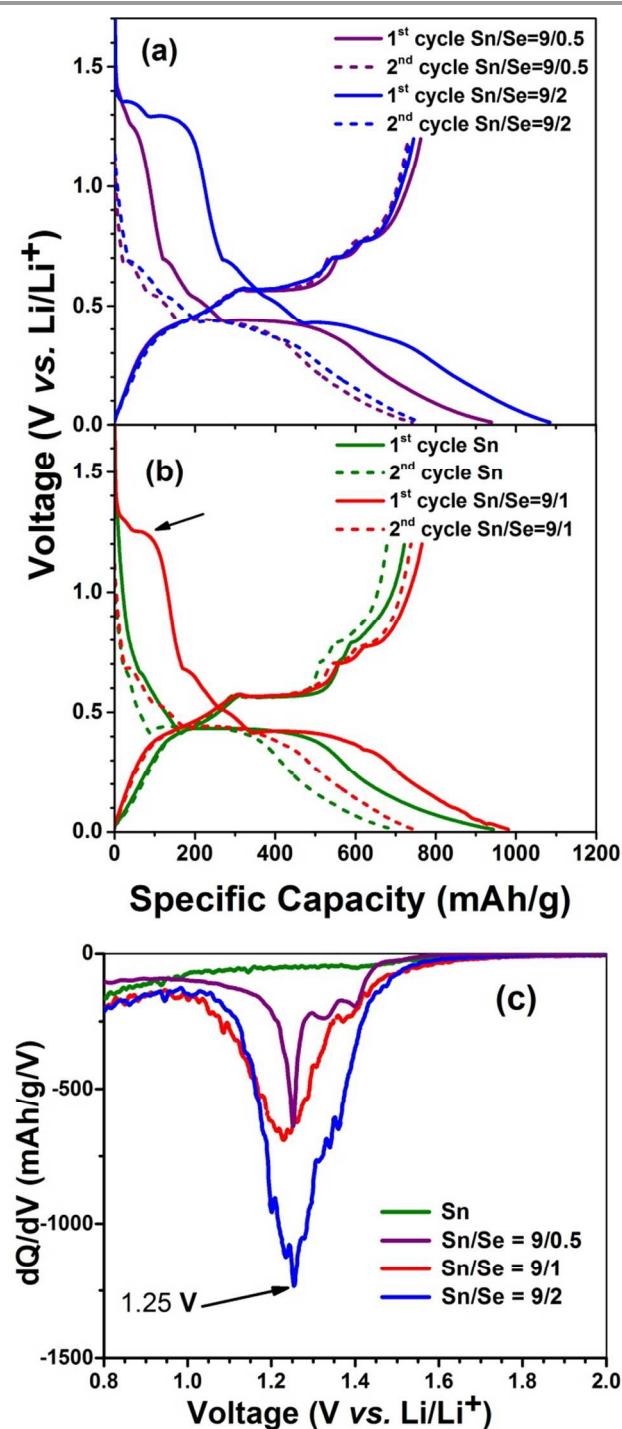


Figure 5. Voltage profiles of electrodes made with (a) Sn/Se(9/0.5) and Sn/Se(9/2), (b) Sn/Se(9/1) and Sn micro-particles. (c) Differential capacity plot for the initial half cycle. All electrodes were cycled at 0.05 C rate (49.6 mA/g).

To further investigate the chemistry occurring during the initial cycle, cyclic voltammetry (CV) with an extended voltage window (from 10 mV to 2.5 V vs. Li/Li⁺) was employed for all electrodes as shown in Fig. 6. Peaks at ~1.3 V and ~1.8 V vs. Li/Li⁺ are observed for all Sn/Se electrodes but not for the Sn electrode. These peaks correspond to the formation and de-

formation of the presumed Li₂Se phase, which is in agreement with the literature on Se^{37,38} and SnSe^{28,39} electrodes tested in a carbonate-based electrolyte. In addition, all peaks associated with the lithiation/delithiation of Sn^{8,36} (Reaction 2) are clearly observed for all electrodes and labelled in Fig 6. These observations lead to the proposed mechanism for Sn/Se anodes as follows:



(Initial charging, ~1.25 V vs. Li/Li⁺)



(Following cycles, potentials as indicated in Figure 6)

Within the cycling voltage window from 10 mV to 1.2 V vs. Li/Li⁺, the initially formed Li₂Se is therefore electrochemically inactive and remains within the Sn/Se electrode during subsequent cycles.

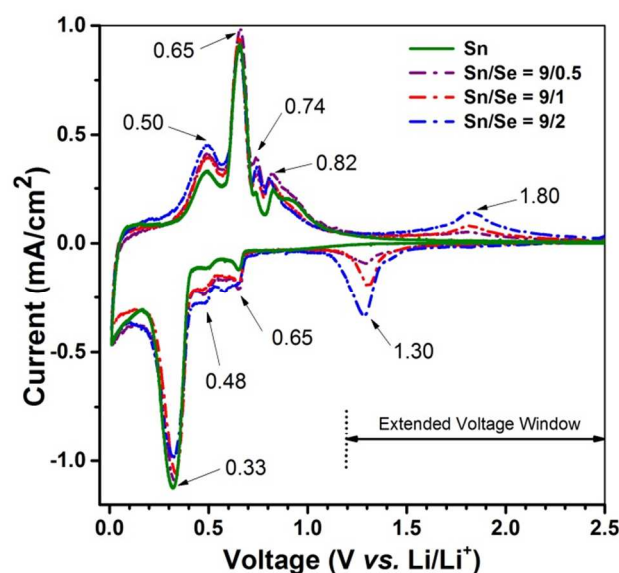


Figure 6. Cyclic voltammograms of the Sn/Se electrodes and of the un-doped Sn electrode at 0.1 mV/s scan rate.

Ex situ XRD spectra of the Sn/Se(9/1) electrode in its (i) pristine, (ii) charged to 100 mV vs. Li/Li⁺ and (iii) discharged to 1.2 V vs. Li/Li⁺ states are shown in Fig. 7. The pristine electrode exhibits the expected Sn and SnSe peaks; in the discharged electrode the Sn peaks are intense, but no SnSe is seen. In the charged, i.e., Li-alloyed, electrode, the intensity of the Sn peaks is greatly reduced but is still observable. The presence of a small metallic tin residue shows that nearly all of the Sn is electroactive, i.e. Li-alloyed. No Li₂Se nor Li_xSn diffraction peaks were observed, indicating that the sizes of their crystallites are too small to diffract, that their phases are nearly or truly amorphous^{38,40} or that an alternative inactive phase formed during the reduction of Se.

The electrochemical evidence for Li₂Se existence, expected from the reduction of Se during the initial charging of Sn/Se, has been shown in Fig. 5 and Fig. 6 which is consistent with the literature regarding stoichiometric SnSe anodes.²⁸ XRD peaks

for the Li_2Se phase, however, are not seen in our ex-situ XRD spectra of the cycled Sn/Se electrodes (see also Figure S3). The lack of an XRD pattern indicating the presence of Li_2Se means that the Se is probably reduced into a non- Li_2Se amorphous material. We speculate that this material might be a more thermodynamically stable Se-containing phase which is truly or nearly amorphous, as has been reported for the reduction products of selenium doped germanium.³³

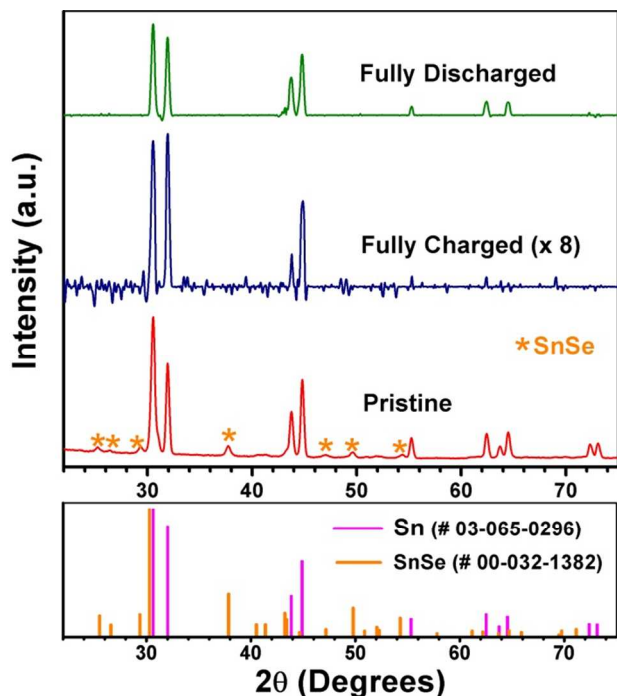


Figure 7. XRD spectra of the pristine, charged and discharged Sn/Se(9/1) electrode.

As shown in Fig. 8 the Sn and Se remain uniformly distributed after the particles are cycled for 100 cycles at a 0.5 C rate. The uniform distribution of Se, and the absence of growth of Li_2Se crystallites to a sufficient size to readily diffract X-rays, as well as the absence of readily observable Li-Sn alloy diffraction peaks suggest that the amorphous or nearly amorphous Li_2Se prevents the growth of large crystalline Li-Sn alloy grains, which would fracture upon cycling.

This observation correlates with XRD characterization of cycled electrodes preserved against air contamination by a Kapton tape covering. In the uncycled microparticles, doped or un-doped, Sn crystals larger than the Sherrer threshold (*c.* 100 nm) were observed. After cycling the electrode (100 cycles at 0.5 C rate) to the discharged state, the Sn within both the Se-doped and un-doped microparticles had re-organized to form a polycrystalline structure with an average grain size of *c.* 50-60 nm. However, it was only for the Se-doped Sn microparticles in which an inactive buffering phase was present that the Sn re-organized into smaller grains without pulverization of the particle into electrically isolated fragments.

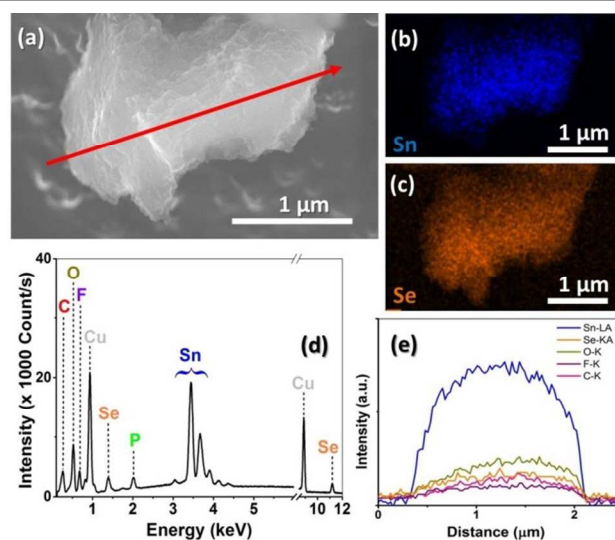


Figure 8. SEM and EDS of a fully discharged Sn/Se(9/1) particle after 100 cycles at 0.5 C rate (496 mA/g). (a) SEM of the EDS-analyzed particle, the red line showing the positions of its EDS scan shown in (e); (b) the Sn distribution (c) the Se distribution; (d) the observed peaks, their assignments and intensities.

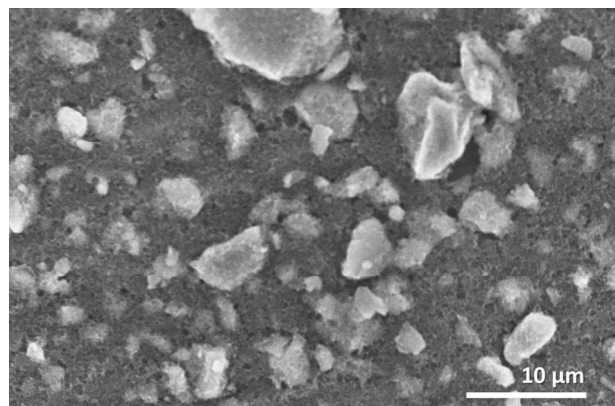


Figure 9. SEM of a fully discharged Sn/Se(9/1) electrode area after 100 cycles at 0.5 C rate (496 mA/g).

Fig. 9 is a SEM image with larger area of the Sn/Se(9/1) electrode after 100 cycles at 0.5 C rate. We observed that the active material microparticles do not fracture upon cycling-associated expansion and contraction, indicating that the network of nanosized grains of Sn formed within the Se-doped Sn anodes during their cycling result in a more mechanically stable material than their un-doped Sn counterparts.

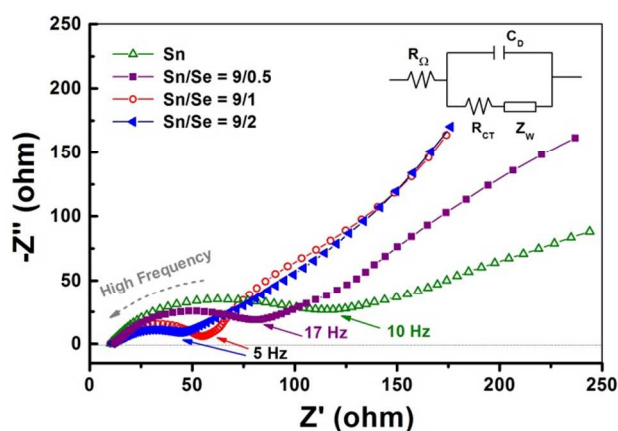


Figure 10. Impedance spectra (Nyquist plots) of the Se-doped and un-doped Sn electrodes after 100 cycles at 0.5 C rate (496 mA/g). The assumed equivalent circuit for the impedances of Table 1 is shown in the insert. Frequency range 100 kHz - 0.05 Hz, 5 mV perturbing voltage.

Table 1. Impedances fitting the spectra of Figure 10 assuming the shown circuit.

Electrode materials	R_{Ω} (Ω)	R_{CT} (Ω)
Sn	12	90
Sn/Se = 9/0.5	13	55
Sn/Se = 9/1.0	12	34
Sn/Se = 9/2.0	11	23

To compare the impedance of Li transport within the different electrode systems, AC impedance spectroscopy was performed for all electrodes at open circuit potentials after 100 cycles at 0.5 C rate (Fig. 10). A sloped line in the low frequency region is related to the mass transfer of Li^+ , and a semicircle in the high frequency region is attributed to a convolution of impedance arising from transport of Li^+ through the SEI and the charge transfer process (represented by R_{CT}). As shown in Table 1, Ohmic resistances (R_{Ω}) of ~ 11 - 13Ω are observed for all electrodes while the charge transfer resistance (R_{CT}) decreases with increasing the Se content of the Sn/Se.

We postulate that the lower resistance to Li^+ transport and charge transfer in the electrodes with richer Se content is attributable to a more stable, thinner SEI forming upon the active material particles. The cycling stability and higher efficiency of the more Se-doped Sn material indicates that these particles do not suffer the magnitude of fracture and pulverization experienced by the pure-Sn particles. This resistance to particle fracture should result in a more stable particle surface and SEI.⁴¹

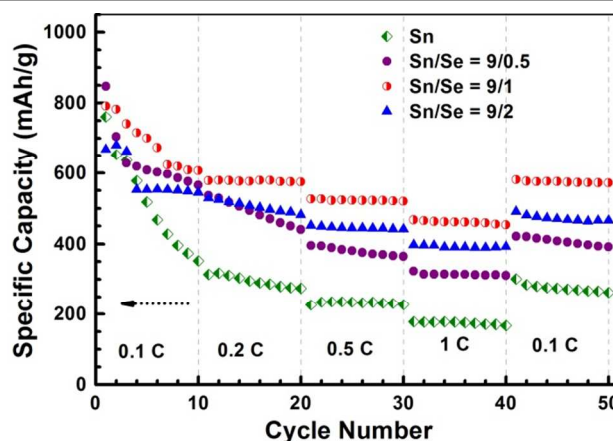


Figure 11. Reversible capacities of electrodes made with Sn/Se and Sn powders, cycled between 10 mV - 1.2 V vs. Li/Li^+ at various C-rates (1 C = 993 mA/g). In computing the specific capacity both the mass of Sn and Se in the electrode were employed.

Fig. 11 shows the reversible capacities of the four electrodes cycled between 10 mV and 1.2 V vs. Li/Li^+ at various C-rates. The rate was increased stepwise from 0.1 C (99.3 mA/g) to 0.2 C, 0.5 C, 1 C then decreased to 0.1 C. The electrodes were cycled for 10 cycles at each rate. The best performing electrode, at any of the C-rates, was the Sn/Se (9/1) electrode. Its retained capacities after cycling at 0.2 C, 0.5 C, 1 C rates are respectively 576, 522 and 461 mAh/g; those of the Sn/Se (9/0.5) electrode are 440, 365 and 311 mAh/g, while those of the un-doped Sn electrode are 290, 233 and 178 mAh/g. The corresponding voltage profiles are found in Supporting Information Figure S3.

Conclusion

Electroactive, micrometer-sized Se-doped Sn particles are produced by the simple and scalable process of quenching from a melt with 9:1 atomic ratio Sn/Se, followed by jet-milling. Lithium battery anodes made of slurry-cast films of these Sn/Se particles vastly outperform in their cycling stability and capacity un-doped Sn particles of similar size. The superior stability of the Se-doped Sn particles is attributed to an amorphous phase of reduced Se formed in the initial charging half cycle. This uniformly distributed phase, likely Li_2Se slows or prevents Li-Sn alloy grain growth, preventing agglomeration of Sn and so avoiding fracture of the micrometer-sized particle upon cycling.

Acknowledgements

The Welch Foundation supported K.C.K., M.L.M., and A.H. through grant F-1131 and C.B.M. through grant F-1436. K.C.K. acknowledges the support of the National Science Foundation through a Graduate Fellowship.

Notes and references

^aMcKetta Department of Chemical Engineering, Department of Chemistry and Biochemistry, Center for Electrochemistry, and Center for Nano- and Molecular Science, University of Texas at Austin

1 University Station, C0400 Austin, TX 78712-0231, United States

^bTexas Materials Institute, University of Texas at Austin

Email: mullins@che.utexas.edu

Electronic Supplementary Information (ESI) available: EDS analysis of Sn/Se(9/2) and Sn/Se(9/0.5); Voltage profiles at various C-rates of Sn and Sn/Se(9/1) electrodes. See DOI: 10.1039/b000000x/

- M. N. Obrovac, L. Christensen, D. B. Le and J. R. Dahn, *J. Electrochem. Soc.*, 2007, **154**, A849-A855.
- S.-C. Chao, Y.-C. Yen, Y.-F. Song, Y.-M. Chen, H.-C. Wu and N.-L. Wu, *Electrochem. Commun.*, 2010, **12**, 234-237.
- I. A. Courtney and J. R. Dahn, *J. Electrochem. Soc.*, 1997, **144**, 2045-2052.
- J. Wang, F. Fan, Y. Liu, K. L. Jungjohann, S. W. Lee, S. X. Mao, X. Liu and T. Zhu, *J. Electrochem. Soc.*, 2014, **161**, F3019-F3024.
- L. Y. Beaulieu, K. W. Eberman, R. L. Turner, L. J. Krause and J. R. Dahn, *Electrochem. Solid-State Lett.*, 2001, **4**, A137-A140.
- L. Xu, C. Kim, A. K. Shukla, A. Dong, T. M. Mattox, D. J. Milliron and J. Cabana, *Nano Lett.*, 2013, **13**, 1800-1805.
- K. Kravchyk, L. Protesescu, M. I. Bodnarchuk, F. Krumeich, M. Yarema, M. Walter, C. Guntlin and M. V. Kovalenko, *J. Am. Chem. Soc.*, 2013, **135**, 4199-4202.
- X. Zhou, J. Bao, Z. Dai and Y.-G. Guo, *J. Phys. Chem. C*, 2013, **117**, 25367-25373.
- R. Yi, F. Dai, M. L. Gordin, S. Chen and D. Wang, *Adv. Energy Mater.*, 2013, **3**, 295-300.
- J. Liu, Q. Zhang, Z.-Y. Wu, J.-T. Li, L. Huang and S.-G. Sun, *ChemElectroChem*, 2015, 611-616.
- A. Cao and A. Manthiram, *Phys. Chem. Chem. Phys.*, 2012, **14**, 6724-6728.
- J. Song, S. Chen, M. Zhou, T. Xu, D. Lv, M. L. Gordin, T. Long, M. Melnyk and D. Wang, *J. Mater. Chem. A*, 2014, **2**, 1257-1262.
- A. S. Arico, P. Bruce, B. Scrosati, J.-M. Tarascon and W. van Schalkwijk, *Nat. Mater.*, 2005, **4**, 366-377.
- J. Wang, W.-L. Song, Z. Wang, L.-Z. Fan and Y. Zhang, *Electrochim. Acta*, 2015, **153**, 468-475.
- D. Deng and J. Y. Lee, *J. Mater. Chem.*, 2010, **20**, 8045-8049.
- Y. S. Jung, K. T. Lee, J. H. Ryu, D. Im and S. M. Oh, *J. Electrochem. Soc.*, 2005, **152**, A1452-A1457.
- K. T. Lee, Y. S. Jung and S. M. Oh, *J. Am. Chem. Soc.*, 2003, **125**, 5652-5653.
- C.-j. Liu, H. Huang, G.-z. Cao, F.-h. Xue, R. A. Paredes Camacho and X.-l. Dong, *Electrochim. Acta*, 2014, **144**, 376-382.
- Y.-M. Lin, P. R. Abel, A. Gupta, J. B. Goodenough, A. Heller and C. B. Mullins, *ACS Appl. Mater. Interfaces*, 2013, **5**, 8273-8277.
- J. Yao, T. Takasaki, K. Nishimura, T. Mukai and T. Sakai, *J. Electrochem. Soc.*, 2013, **160**, A980-A984.
- X. Fan, P. Dou, A. Jiang, D. Ma and X. Xu, *ACS Appl. Mater. Interfaces*, 2014, **6**, 22282-22288.
- R. Zhang and M. S. Whittingham, *Electrochem. Solid-State Lett.*, 2010, **13**, A184-A187.
- P. R. Abel, M. G. Fields, A. Heller and C. B. Mullins, *ACS Appl. Mater. Interfaces*, 2014, **6**, 15860-15867.
- M. I. Bodnarchuk, K. V. Kravchyk, F. Krumeich, S. Wang and M. V. Kovalenko, *ACS Nano*, 2014, **8**, 2360-2368.
- S. Fan, L. Y. Lim, Y. Y. Tay, S. S. Pramana, X. Rui, M. K. Samani, Q. Yan, B. K. Tay, M. F. Toney and H. H. Hng, *J. Mater. Chem. A*, 2013, **1**, 14577-14585.
- Y. Kim, Y. Kim, Y. Park, Y. N. Jo, Y.-J. Kim, N.-S. Choi and K. T. Lee, *Chem. Commun. (Cambridge, U. K.)*, 2015, **51**, 50-53.
- X. Wang, B. Liu, Q. Xiang, Q. Wang, X. Hou, D. Chen and G. Shen, *ChemSusChem*, 2014, **7**, 308-313.
- H. S. Im, Y. R. Lim, Y. J. Cho, J. Park, E. H. Cha and H. S. Kang, *J. Phys. Chem. C*, 2014, **118**, 21884-21888.
- P. K. Dutta, U. K. Sen and S. Mitra, *RSC Advances*, 2014, **4**, 43155-43159.
- L. Wu, X. Hu, J. Qian, F. Pei, F. Wu, R. Mao, X. Ai, H. Yang and Y. Cao, *J. Mater. Chem. A*, 2013, **1**, 7181-7184.
- JET PULVERIZER WORKS TO COMMERCIALIZE EMERGING LITHIUM-ION BATTERY TECHNOLOGY, <http://www.jetpulverizer.com/news-and-events/article01.php>.
- P. R. Abel, K. C. Klavetter, A. Heller and C. B. Mullins, *J. Phys. Chem. C*, 2014, **118**, 17407-17412.
- K. C. Klavetter, J. Pedro de Souza, A. Heller and C. B. Mullins, *J. Mater. Chem. A*, 2015.
- Y.-M. Lin, P. R. Abel, A. Heller and C. B. Mullins, *J. Phys. Chem. Lett.*, 2011, **2**, 2885-2891.
- O. H., *J. Phase Equilib.*, 1998, **19**, 293.
- M. Winter and J. O. Besenhard, *Electrochim. Acta*, 1999, **45**, 31-50.
- H. Wang, S. Li, Z. Chen, H. K. Liu and Z. Guo, *RSC Advances*, 2014, **4**, 61673-61678.
- Y. Cui, A. Abouimrane, C.-J. Sun, Y. Ren and K. Amine, *Chem. Commun. (Cambridge, U. K.)*, 2014, **50**, 5576-5579.
- M.-Z. Xue, J. Yao, S.-C. Cheng and Z.-W. Fu, *J. Electrochem. Soc.*, 2006, **153**, A270-A274.
- S.-C. Chao, Y.-F. Song, C.-C. Wang, H.-S. Sheu, H.-C. Wu and N.-L. Wu, *J. Phys. Chem. C*, 2011, **115**, 22040-22047.
- M. B. Pinson and M. Z. Bazant, *J. Electrochem. Soc.*, 2013, **160**, A243-A250.